Adsorption (2009) 15: 1–12
DOI 10.1007/s10450-009-9154-0

Behavior of ethylene and ethane within single-walled carbon nanotubes. 1-Adsorption and equilibrium properties

Fernando J.A.L. Cruz · Erich A. Müller

Received: 20 March 2008 / Revised: 13 January 2009 / Accepted: 9 February 2009 / Published online: 28 February 2009

Abstract Endohedral adsorption properties of ethylene and ethane onto single-walled carbon nanotubes were investigated using a united atom (2CLJQ) and a fully atomistic (AA-OPLS) force fields, by Grand Canonical Monte Carlo and Molecular Dynamics techniques. Pure fluids were studied at room temperature, $T = 300$ K, and in the pressure ranges $4 \times 10^{-4} < p < 47.1$ bar (C_2H_4) and $4 \times 10^{-4} < p < 37.9$ bar (C_2H_6). In the low pressure region, isotherms differ quantitatively depending on the intermolecular potential used, but show the same qualitative features. Both potentials predict that ethane is preferentially adsorbed at low pressures, and the opposite behavior was observed at high loadings. Isosteric heats of adsorption and estimates of low pressure Henry's constants, confirmed that ethane adsorption is the thermodynamically favored process at low pressures. Binary mixtures of C_2H_4/C_2H_6 were studied under several (p, T) conditions and the corresponding selectivities towards ethane, S, were evaluated. Small values of $S < 4$ were found in all cases studied. Nanotube geometry plays a minor role on the adsorption properties, which seem to be driven at lower pressures primarily by the larger affinity of the alkane towards the carbon surface and at higher pressures by molecular volume and packing effects. The fact that the selectivity towards ethane is similar to that found earlier on carbon slit pores and larger diameter nanotubes points to the fact that the peculiar 1-D geometry of the nanotubes provides no particular incentive for the adsorption of either species.

F.J.A.L. Cruz · E.A. Müller (✉)
Department of Chemical Engineering, Imperial College London, South Kensington Campus, London SW7 2AZ, UK
e-mail: e.muller@imperial.ac.uk

Keywords Adsorption · Molecular simulation · Carbon nanotubes · Ethylene · Ethane · Grand canonical Monte Carlo · Molecular dynamics

1 Introduction

Separations of close boiling point mixtures, such as the ethylene/ethane mixture, are amongst the most energy-intensive unit operations in chemical and petrochemical plants, where they usually involve low-temperature distillation techniques. For this type of separations, encompassing structurally and/or energetically similar molecules, alternative techniques are actively sought, particularly for small-scale applications such as those used in the pharmaceutical, biomedical and aerospace industry (Noble and Agrawal 2005). While adsorption using nanoporous materials is posed to be considered as an option, our current molecular-level knowledge of the physical phenomena involved in the adsorption and diffusion of fluids in confined nanospaces still needs improvement.

Molecular simulation has played a key role in understanding the intricate details of the cooperative adsorption of ethane and ethylene. To date, two types of adsorbents have been proposed for the separation of this kind of mixtures; zeolites (Al-Baghli and Loughlin 2006; Da Silva and Rodrigues 1999) and π-complexation sorbents (Yang 2003). The separation using zeolites is kinetic in nature, i.e. the separation is based on the distinct diffusivities of the species. On the other hand, π-complexation sorbents are designed by doping conventional adsorbents with cations (usually Cu^+ or Ag^+) that have a high affinity with the double bond present in alkenes. While selectivity in these latter adsorbents is high, regeneration of the adsorbent is an issue if continuous processing is required. In this context, the quest

for a carbon adsorbent, suitable for this type of separation, would prove to be an attractive alternative, on basis of cost, availability and practicability. The adsorption of ethane and ethylene onto activated microporous carbon has been already discussed (Cracknell and Nicholson 1994; Do and Do 2004a, 2004b; Klochko et al. 1999), and the competitive adsorption of a mixture of both has been studied by Do and Do (2005) using a united-atom force field. Recently, we have addressed the possibility of separating an ethylene/ethane mixture using an ideal carbon slit pore as the adsorption media (Curbelo and Müller 2005). Preliminary results obtained using molecular simulations seemed to suggest this separation is feasible using adsorption, as selectivity values of the order of five (or higher) were characteristic under the pressure and temperature conditions considered. Recently, Guo et al. (2007) have employed gas-chromatography to monitor the co-adsorption of C_2H_4/C_2H_6 mixtures on various activated carbons. Their findings suggest that the strongly-adsorbed component (ethane) could replace the weakly-adsorbed component (ethylene), and the adsorption capacities of the hydrocarbon gas mixtures onto the activated carbons are between that of pure ethane and pure ethylene.

Since their first laboratory preparation in the early 90's (Bethune et al. 1993; Iijima 1991; Iijima and Ichihashi 1993), carbon nanotubes have attracted a considerable amount of attention due to their unique and exciting new features, such as optical (Fagan et al. 2007) and electronic properties (Taherpour 2007). Recently (Lu et al. 2006), a method has been developed to fine tune a nanotube diameter that can afterwards be purified according to different needs and strategies (Liu et al. 2007; Yerushalmi-Rozen and Szleifer 2006). Their structure can be rationalized as resulting from the folding of a graphene sheet, or several of them aligned in a concentric way, giving rise respectively to single-walled carbon nanotubes (SWCNTs) or multi-walled carbon nanotubes (MWCNTs). The graphene folding along a specific directional vector (n, m) will produce a zig-zag $(n, 0)$, arm-chair (m, m), or chiral (n, m) nanotube (Meyyappan 2005). Similarly to what happens to molecules inside other confining environments, the restricted space within SWCNT is expected to induce phase changes and local behavior which may not have a parallel in the fluids bulk phases (Alba-Simionesco et al. 2006; Gelb et al. 1999). Therefore, it is not surprising that along with other confining nanosurfaces, SWCNTs are being actively investigated (Bekyarova et al. 2003; Darkrim et al. 2002) and, in spite of the current cost and difficulties to mass-produce them, are being considered as possible storage nanomaterials for H_2 and CH_4, building blocks in composites (Sinnott and Andrews 2001), chemical sensors (Hong et al. 2007), and separating agents of organic vapors (Jiang et al. 2005; Jiang and Sandler 2006; Mao and Sinnott 2001), amongst other uses. Recently, Funk et al. (2007) employed molecular beam scattering experiments to throw some light onto the adsorption of *n*/*iso*-butane on SWCNTs. Kondratyuk et al. (2005) have studied a similar system, performing molecular dynamics simulations, and determining the adsorption profiles of *n*-heptane on the interior and exterior walls of a nanotube bundle; the fluid molecules were described according to a united-atom model, and the self-diffusion properties have been characterized at different temperatures. A similar fluid force-field was used by Agnihotri et al. (2006) in their Grand Canonical Monte Carlo simulations. In this last work, the authors have described the endo- and exohedral adsorption profiles of hexane, modeling the nanotube as a structureless nanocylinder of infinite length.

The present work aims to extend our knowledge regarding the adsorption and separation of ethylene, ethane, and their corresponding binary mixtures, when the fluids are put in contact with an adsorbent made of a zig-zag type (16, 0) SWCNT. We have employed both a detailed all-atom description and a coarse-grained version of the intermolecular potentials for the fluids and described the adsorbent explicitly, as detailed in the next section. We have used both classical molecular dynamics (MD) in a canonical ensemble, and grand canonical Monte Carlo (GCMC) simulations. A following paper will complement these results with dynamical information on the diffusion processes within these confined spaces.

2 Force fields and models

The outcome of any simulation study is directly related to the confidence placed in the applicability and accuracy of the intermolecular potentials used. In general, it is assumed that the more detailed the intermolecular potential, the more confident one can be on the results obtained from it. The downside is that complexity is usually synonymous of increased computational requirements, sometimes to the extent of rendering the simulations unfeasible or producing spurious results; e.g. in macromolecular science, simplified coarse grained potentials perform and describe the physical behavior better than the detailed atomistic ones since they allow the observation of longer-lived processes, avoiding metastable non-equilibrated states. In the present paper we directly compare two models, a well known fully atomistic detailed potential (AA-OPLS) and a coarse grained model (2CLJQ) which has been successful in other applications, neither of whose performance in this context has been evaluated.

2.1 All-atom (AA) OPLS

The all-atom (AA) OPLS parameterization of Jorgensen et al. (1996) is employed here for both the inter- and intramolecular interactions. Within the AA model, all the

atoms in the fluid molecules are modeled as Lennard-Jones (LJ) spheres (1). Explicit electrostatic charges, q_i, were considered for all particles. In order to take into account the 1–4 nonbonded interactions, an appropriate scaling-factor, $f_{ij} = 0.5$, was used (as opposed to fixing $f_{ij} = 1.0$ for all other cases), thus allowing the AA-OPLS parameterization to be employed for both the inter- and intramolecular interactions.

$$U(r_{ij}) = \sum_i \sum_j \left\{ \frac{q_i q_j e^2}{r_{ij}} + 4\varepsilon_{ij}\left[\left(\frac{\sigma_{ij}}{r_{ij}}\right)^{12} - \left(\frac{\sigma_{ij}}{r_{ij}}\right)^{6}\right]\right\} f_{ij} \tag{1}$$

Both ethylene and ethane models included explicit contributions from bond stretching (2), angle bending (3) and dihedral energies (4); K_i and V^i_{1-3} are the corresponding force constants.

$$U_{bonds} = \sum_{bonds} K_r (r - r_{eq})^2, \tag{2}$$

$$U_{angles} = \sum_{angles} K_\theta (\theta - \theta_{eq})^2, \tag{3}$$

$$U(\phi) = \sum_i \frac{V^i_1}{2}[1 + \cos(\phi)] + \frac{V^i_2}{2}[1 - \cos(2\phi)] + \frac{V^i_3}{2}[1 + \cos(3\phi)] \tag{4}$$

The fluid molecular geometry, namely equilibrium bond lengths and angles, and the corresponding parameters, r_{eq}, θ_{eq}, have been obtained from the standard literature values (Jorgensen et al. 1996; McDonald et al. 1997) and were adopted without further refinement. The parameter values are summarized in Tables 1a, 1b.

Table 1a AA-OPLS Lennard-Jones force field parameters (1)

	q_i	ε_{ii}/K	σ_{ii}/Å
C_2[a]	−0.230	38.270	3.55
H_2[a]	0.115	15.107	2.42
C_3[a]	−0.180	33.235	3.50
H_3[a]	0.060	15.107	2.50

[a]C_2 and H_2, and C_3 and H_3 are the carbon and hydrogen atoms of ethylene and ethane, respectively

Table 1b AA-OPLS bond stretching (2) and angle bending parameters (3)

	r_{eq}/Å	K_r/K		θ_{eq}/°	K_θ/K
C_2–C_2[a]	1.340	549.0	H_2–C_2–H_2	117.0	35
C_2–H_2[a]	1.080	340.0	H_2–C_2–C_2	117.0	35
C_3–C_3[a]	1.526	310.0	H_3–C_3–H_3	109.5	35
C_3–H_3[a]	1.090	331.0	H_3–C_3–C_3	109.5	35

[a]Coefficients for the torsional energies (4): V_2 (H_2–C_2–C_2–H_2) = 58.6152 kJ mol^{-1}, V_3 (H_3–C_3–C_3–H_3) = 1.3314 kJ mol^{-1}

2.2 2CLJQ

Recently, Vrabec et al. (2001) have parameterized a large number of small organic molecules using a coarse grained potential based on a Lennard-Jones dumbbell of variable bond length, L, which may or may not have an embedded centrally located multipole moment (dipole, quadrupole, etc.). In the case that concerns us here, both ethane and ethylene have been considered as a two center uncharged LJ molecule with a quadrupole moment placed at the center of mass (2CLJQ). This particular force field has been used to study and predict vapor liquid equilibria in mixtures (Stoll et al. 2003), transport properties (Fernández et al. 2005a, 2005b), derivative thermodynamic properties such as Joule-Thomson inversion curves (Chacin et al. 1999; Vrabec et al. 2005) and has been used in adsorption studies (Curbelo and Müller 2005). Briefly, the overall energy is given by the sum of the Lennard-Jones and quadrupolar interactions (5) (Gray and Gubbins 1984).

$$U(r_{ij}, r_{ab}) = \sum_i \sum_j 4\varepsilon_{ij}\left[\left(\frac{\sigma_{ij}}{r_{ij}}\right)^{12} - \left(\frac{\sigma_{ij}}{r_{ij}}\right)^{6}\right] + \frac{3}{4}\frac{Q^2}{(4\pi\varepsilon_0) r^5_{ab}}[1 - 5(c_i^2 + c_j^2) - 15c_i^2 c_j^2 + 2(c - 5c_i c_j)^2] \tag{5}$$

In this formulation, i and j refer to the LJ sites on the molecules, r_{ab} is the centre-centre distance amongst molecules, r_{ij} is the distance between the centers of molecules i and j, $c_i = \cos\theta_i$, $c_j = \cos\theta_j$, and $c = \cos\theta_i \cos\theta_j + \sin\theta_i \sin\theta_j \cos\phi_{ij}$, where θ_i and θ_j are the polar angles of the molecular axis with respect to a line joining the molecular centers, ϕ_{ij} is the difference in the azimuthal angles and ε_0 is the vacuum permittivity (8.85419×10^{-12} C^2/N m^{-2}). The fluid-fluid parameters are taken directly from the parameterization of Vrabec et al. (Table 2) and give a quantitative representation of both the equilibrium vapor-liquid coexisting bulk densities and the P–V–T behavior of the fluid phases (Vrabec et al. 2001).

The 2CLJQ model has already proven to be efficient when dealing with bulk binary mixtures of the type being studied here, exhibiting a very good agreement with experimental VLE data without the need to use any binary interaction parameters (Carrero-Mantilla and Llano-Restrepo 2003).

Table 2 2CLJQ parameters (5) (Vrabec et al. 2001)

	ε_{ii}/K	σ_{ii}/Å	L/Å	Q/B
CH_2[a]	76.95	3.7607	1.2695	4.331
CH_3[a]	136.99	3.4896	2.3762	0.8277

[a]CH_2 and CH_3 are the united atom LJ sites for ethylene and ethane, respectively

2.3 Carbon nanotubes

SWCNTs are described in an atomistic way, assuming carbon atoms to be a collection of discrete Lennard-Jones spheres, with parameters, $\varepsilon_{CRT} = 28.0$ K and $\sigma_{CRT} = 3.4$ Å (Steele 1973, 1974, 1993). The nanotube walls are therefore rigid and corrugated, i.e., all atoms in the tube are explicitly included in the calculations. Nanotube corrugation and geometry is unlikely to have any effect on the equilibrium properties studied, since the temperatures involved are far above the expected solid-fluid transitions of the bulk fluids. Johnson and co-workers (Ackerman et al. 2003) have presented detailed analysis which concludes that for studies of adsorption and transport behavior within SWCNTs, the potential should optimally be an atomistic description with rigid bonding, as the one being employed in the present work. Additionally, comparison of computer simulations with adsorption experiments of Xe on nanotubes suggests that the potentials developed for graphene sheets may be transferred to the case of cylindrical pores (Simonyan et al. 2001).

In a planar graphene sheet, carbon atoms are sp^2 hybridized, with an overall charge distribution of electrical quadrupoles located perpendicular to the surface. When this sheet is bended to produce a nanotube, the sp^2 orbitals tend to be "squeezed-out" towards the tube outer space, and therefore the original quadrupole moments will be dislocated further away from the tube's interior volume (Meyyappan 2005). As the nanotube radius decreases (due to the increased bending of the original graphene plane) this effect tends to be more pronounced and confined molecules will experience a reduced charge anisotropy. Additionally, SWCNT chirality also has an effect on the electronic structure, as it can render the tubes to be metallic or semi-metallic and this might have an effect on the interactions between adsorbents and adsorbates. It is not clear what the effect of these contributions would be. At the (high) temperature being studied here, the neglect of any quadrupole-surface interactions seems adequate (Kaneko et al. 1994). Thus, we have excluded contributions arising from the quadrupole moment that could be ascribed to the solid walls. This simplification has been frequently adopted by previous studies dealing with isolated nanotubes and nanotubes bundled in membranes (Heyden et al. 2002; Hung et al. 2005; Kondratyuk et al. 2005; Mukherjee et al. 2007; Skoulidas et al. 2006; Striolo et al. 2005), and has a parallel on the approximations made when studying adsorption on graphene sheets (Sweatman et al. 2006; Vernov and Steele 1992; Zhao and Johnson 2005). Even in scenarios where these contributions are expected to be important, as in the case of hydrogen adsorption onto single-walled nanotubes, Simonyan et al. (1999) concluded that the presence of charges on the nanotube walls leads to an increase of only around 15% on the adsorption capacity at $T = 298$ K. Following the above discussed directives, we have used zig-zag type single-walled carbon nanotubes, $(n, 0)$ (Meyyappan 2005; Saito et al. 1998) with $n = 16$ and a length to diameter ratio of $(L/D) \approx 5.67$. An armchair, (9, 9), and a chiral, (12, 6), nanotubes have also been considered. As previously mentioned, the bending of a planar graphene sheet to originate a carbon nanotube results in the squeezing-out of the π clouds towards the nanotube exterior volume. This same effect will tend to increase the purely sp^2 hybridized σ (C–C) bond, 1.4 Å. In the simulations, we have considered a value of 1.42 Å for the C–C sigma bond. This latter bond length has been previously used to study the adsorption and diffusive behavior of model fluids in carbon nanotubes (Düren et al. 2002; Jiang et al. 2004).

In all cases, cross fluid-fluid and solid-fluid interaction parameters $(\sigma_{ij}, \varepsilon_{ij})$ have been calculated according to the classical Lorentz-Berthelot combining rules (Allen and Tildesley 1990; Rowlinson and Swinton 1982), $\sigma_{ij} = (\sigma_{ii} + \sigma_{jj})/2$, $\varepsilon_{ij} = (\varepsilon_{ii} \cdot \varepsilon_{jj})^{1/2}$, and no attempt has been made to adjust them, as no reliable experimental data is available.

The surface potential employed involves some simplifications with regard to the lack of flexibility (breathing) of the surface, the validity of the direct application of the fluid-fluid and cross parameters to the adsorption process, the absence of end-effects (open-ended nanotubes), amongst others. One must bear in mind that any of the aforementioned assumptions may have an effect on the results, so a direct comparison of the simulation results with experiments should be made with care. Furthermore, actual experimental adsorption isotherms involve both exohedral and endohedral adsorption and suffer from issues such as poor purity of samples and polydispersity of the nanotubes diameters. A critical review of the limitations of the simulation models is available elsewhere (Steele 1993).

In order to relate the results obtained from the simulations to macroscopical observed quantities, we arbitrarily define an internal tube diameter accessible to fluid molecules, D_{eff}, and relate this quantity with the physical diameter as measured from the center of the carbon atoms, D. We will assume that the accessible volume for the fluid is given by $D_{eff} = D - \sigma_{CRT}$, where σ_{CRT} is the Lennard-Jones diameter of a graphitic carbon atom (3.4 Å). This

definition has no effect whatsoever on the molecular simulation calculations. The calculation of the available volume can be later refined, for example, introducing a distance of closest approach between a fluid molecule and the carbon atoms on the solid wall (Kaneko et al. 1994; Ohba and Kaneko 2002), enabling direct comparisons with experimental data (Cruz and Müller 2008, unpublished results).

3 Simulation details

3.1 Molecular dynamics

Classical molecular dynamics simulations were performed using the DL_POLY 2.16 package (Smith and Todorov 2006). The Verlet algorithm was used to integrate the equations of motion (van Gunsteren and Berendsen 1990; Verlet 1967), the Ewald summation method was employed to calculate the long-range electrostatic interactions for the fluid (van Gunsteren and Berendsen 1990; Woodcock and Singer 1971), and the Nosé-Hoover thermostat was used to control the temperature (Nosé 1984). All runs were performed setting the thermostat for $T = 300$ K under the canonical ensemble (NVT), and spanning a pressure range of $0.6 < p < 26$ bar and $0.28 < p < 24.5$ bar, for ethylene and ethane, respectively. A potential cut-off distance of 15 Å and a time step of $t = 1$ fs were used.

Large-scale simulations were set up in an elongated box, where an open-ended SWCNT was exposed to a bulk fluid contained within it. Short-range repulsive walls were placed at the tube's openings to prevent exohedral adsorption (Fig. 1). A similar set-up has recently been employed by Longhurst and Quirke (2007) to study the temperature driven pumping of fluids through nanotubes. It should be noted that the bulk fluid was previously equilibrated at $T = 300$ K for at least 0.1 ns; this procedure allowed for the thermal stabilization of the bulk fluids, with temperature fluctuations always less than 10%, and in most cases less than 5%. In order to study different bulk fluid pressures (densities), two different simulation boxes have been built, $(30 \times 30 \times 300)$ Å, and $(60 \times 60 \times 300)$ Å, with periodic boundary conditions in x–y–z space. In these simulations, the AA-OPLS potential was used for the fluids.

The non-equilibrium diffusion into the pore was monitored until steady state conditions were attained, and the corresponding endohedral adsorption was recorded. Statistics of the whole system have been registered up to 0.8–3 ns, depending on the bulk fluid pressure. In Fig. 2 we present snapshots of two different pressure simulations with

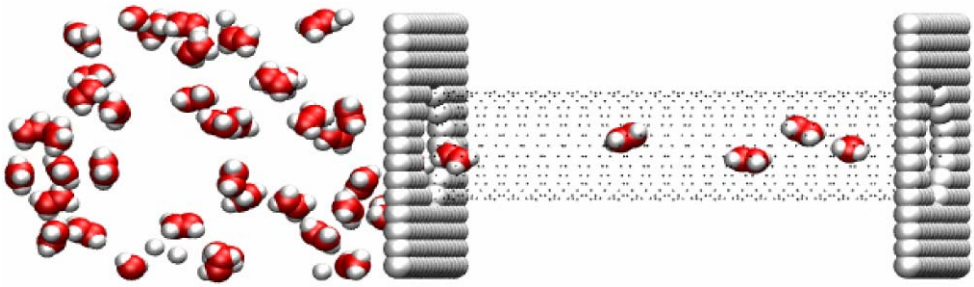

Fig. 1 Simulation box set-up used in the MD calculations: ethylene (*red*), repulsive walls (*white*). The zig-zag SWCNT (16, 0) is represented as a mesh of carbon atoms (*black*)

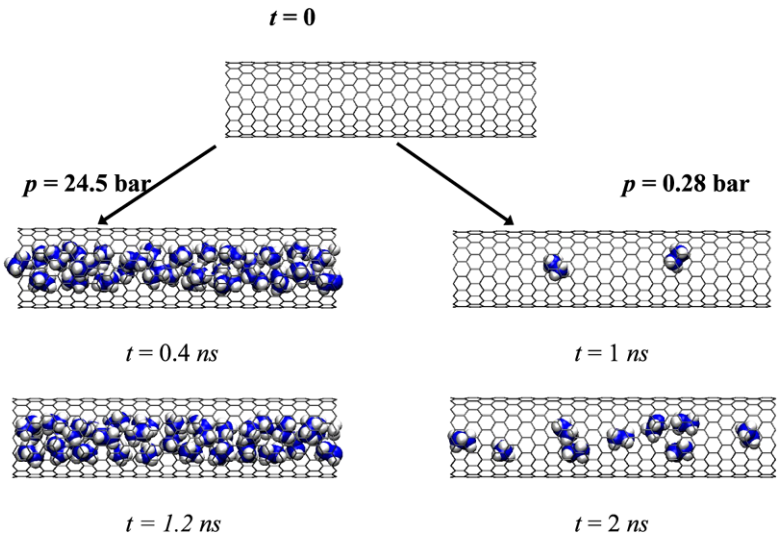

Fig. 2 Snapshots of bulk ethane, at $T = 300$ K, in contact with a zig-zag SWCNT (16, 0) as a function of time for two different final bulk pressures (shown). Coexisting bulk fluid is omitted for clarity

ethane in contact with a nanotube. The highest (final) pressure fluid ($p = 24.5$ bar) needs only about 0.4 ns to achieve steady-state, and from there onwards only minor equilibrium fluctuations were registered. In the low pressure simulation ($p = 0.28$ bar), even at $t = 1$ ns the system is still away from equilibrium, reaching this final state only after a total simulation time of ca. 2 ns.

The corresponding pressure of the bulk fluid in equilibrium with the confined adsorbed phase is calculated by relating the density of the bulk fluid to the pressure using standard equations of state (NIST 2008).

3.2 Grand canonical Monte Carlo

We have used Grand Canonical Monte Carlo simulations (GCMC) as detailed in standard references (Allen and Tildesley 1990; Frenkel and Smit 2002; Nicholson and Parsonage 1982). The Grand Canonical ensemble allows the equilibration of a gas phase with a confined fluid phase and in that sense it is an ideal technique to study adsorption. In GCMC the temperature, T, the volume of the pore, V, and the chemical potential of each species, μ, are kept constant throughout the simulation. The number of molecules in the pore is allowed to vary, and its statistical average is the relevant quantity of interest. In our simulations we have replaced the chemical potential by the more convenient variable, activity (Leach 1996), $\zeta_i = \Lambda^{-3} \exp(\mu / k_B T)$, which has the advantage of corresponding to the number density in the ideal gas limit. Λ is the De Broglie wavelength, and k_B is the Boltzmann's constant. Activity can be directly related to vapor pressures using a truncated virial equation of state, $p = RT\zeta_i(1 - B\zeta_i)$, where B is the second virial coefficient and is available from reported correlations as a function of temperature for the pure components (Daubert and Danner 1994). In the simulations of mixtures we have assumed an ideal solution behavior, and calculated the total pressure as the sum of the two partial pressures of ethylene and ethane. The 2CLJQ fluid model was used in the GCMC simulations. Fluid-fluid potentials were cutoff at 20 Å and no long-range corrections were included. We have used an elongated simulation cell, ($25 \times 25 \times 54$) Å and only considered endohedral adsorption unto a single nanotube. Simulations were run for a total of 30×10^6 GCMC cycles. The systems were started up with an empty pore and filled up until an equilibrium condition was attained. Each Grand Canonical Monte Carlo cycle consists of the movement of a randomly chosen molecule, which is either a displacement of its center of mass or a rotation about it and a random attempt to either create or destroy molecules. Maximum displacements and rotations were adjusted to obtain approximately a 30% acceptance ratio.

Pure fluid simulations were conducted at $T = 300$ K and within a pressure range of $4 \times 10^{-4} < p < 47.1$ bar and $4 \times 10^{-4} < p < 37.9$ bar, for ethylene and ethane, respectively. In order to study the selectivity behavior towards equimolar mixtures of C_2H_4/C_2H_6, adsorption runs were performed at two different temperatures, $T = 300$ K, and $T = 400$ K. To mimic a characteristic refinery feedstock we have also simulated a mixture composed of 90% ethylene doped with 10 mol% ethane in a temperature range of $260\ \text{K} < T < 450$ K.

Although two distinct simulation methods are employed, given the same conditions, they produce congruent results for the adsorption and we have used both methods as complementary tools. End effects, present in the MD simulations where the nanotube is in contact with a bulk fluid, can be discarded by taking the appropriate average loading in the central part of the tube. GCMC effectively avoids this problem by considering an infinitely long nanotube. Furthermore, GCMC simulations are computationally much more efficient, as they do not need to cocurrently model the bulk fluid. However, GCMC fails to provide dynamical information. The results corresponding to the non-equilibrium and diffusion properties of these systems are to be published in the second part of this paper and thus not included herein.

4 Results and discussion

4.1 Pure fluids

The adsorption isotherms obtained from the two distinct intermolecular potentials used for the fluid-fluid interactions are recorded in Fig. 3. The results are shown for the adsorption of pure ethylene and ethane onto a (16, 0) SWCNT at $T = 300$ K. Surface coverage data results from a statistical analysis of the average number of endohedrally adsorbed molecules. The AA-OPLS data shows a slightly larger scattering due to the intrinsically dynamical nature of the MD calculations employed. It is evident from the isotherms that the AA-OPLS and the 2CLJQ potentials disagree in a quantitative manner; however they exhibit the same qualitative trends. Both C_2H_4 and C_2H_6 adsorption capacities seem higher when using the 2CLJQ model. The differences between the AA-OPLS and the 2CLJQ models are more pronounced for the ethane molecule than for ethylene. This may be due to the fact that the 2CLJQ force field forces assumes a rigid behavior between the united atom centers, and while for C_2H_4 this a good approximation to the real molecule, in the case of C_2H_6, this does not account for vibrations and/or torsions about the C–C bond thus neglecting the eventual switch between the most stable conformations for the molecule, eclipsed and staggered (Solomons 1992). Similarly, the charge distribution for ethane is not as static as that for ethylene, so a fixed value of a quadrupole moment may also be a source of discrepancy. Furthermore, both potential models

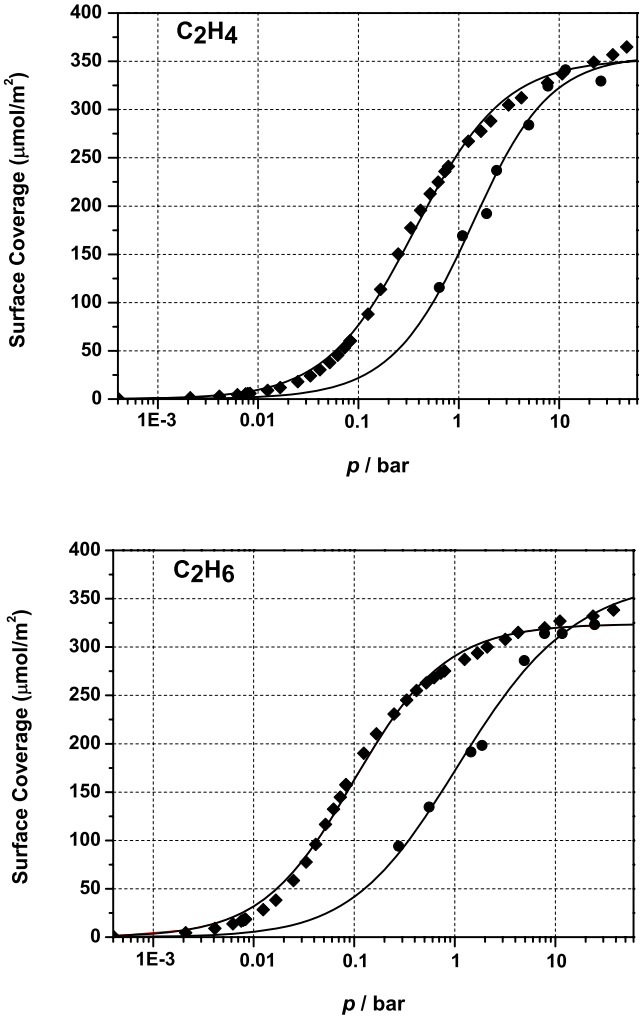

Fig. 3 Adsorption isotherms of pure ethylene and ethane onto (16, 0) SWCNT at $T = 300$ K; Statistical uncertainties are reflected in the symbols' size. *Circles* are AA–OPLS, *diamonds* are 2CLJQ. *Lines* are a fit using the Toth isotherm (7). Raw simulation data available from the corresponding author upon request

are effective pair potentials fitted to fluid phase data (densities, vapor-liquid equilibria), so their reliability in terms of adsorption is only an extrapolation. It is not surprising then that the low pressure region, where solid-fluid interactions dominate, exhibits the larges discrepancies between the models. As pressure surpasses a threshold, c.a. 10 bar, both force fields seem to predict similar adsorption capacities in the ranges studied; in this region, the molecules are rather well packed.

The adsorption curves belong to type-I isotherms, according to the IUPAC classification (IUPAC 1985). They are initially concave regarding the p axis, indicating the formation of an adsorbed layer whose thickness increases progressively with increased pressure. An immediate conclusion is the fact that in the low pressure region ($p < 3$ bar), alkane molecules are more adsorbed than their unsaturated analogs. This is in agreement with recent simulation data from Keil and Jakobtorweihen (2007) for the adsorption of a series of alkanes and alkenes in (20, 0)–(40, 0) nanotubes. As ethane possesses a larger dispersive interaction than ethylene, it is natural for the molecule to become the preferential adsorbing species, in a pressure range where energetic interactions with the solid walls govern the adsorption process. As pressure increases, around $3 < p < 6$ bar, there seems to be a cross over point on the curves, and henceforward ethylene plays the role of the preferentially adsorbed species. At high pressures the dominant aspect ruling over adsorption is apparently an entropic factor, related to the packing efficiency of molecules; it is reasonable to assume that a smaller molecule (ethylene) is able to better accommodate inside the nanotube than a larger one (ethane). This general occupancy tendency and the cross-over just mentioned have also been observed in experimental data for ethylene and ethane adsorption onto activated carbons (Choi et al. 2003) and in GCMC simulations of the same fluids in carbon slit-pores (Curbelo and Müller 2005).

Inspection of the snapshots at intermediate configurations during the MD simulations gives some insight onto the adsorption process (Fig. 4). At low bulk pressures ($p = 0.28$ bar), only a partial monolayer coverage is observed and new molecules entering the confined space will tend to assemble themselves around the inner walls. With pressure increase, the internal loading follows the same trend and surface coverage approaches completion; after $p \approx 11$ bar, no significant change could be observed in the nanotube loading.

In terms of computational efficiency, as expected, the coarse grained 2CLJQ potential requires an order of magnitude less computer time, and is significantly simpler from the point of view of coding the program. Ewald summations, necessary to account for the explicit charges in the AA-OPLS model, are unnecessary in the case of the 2CLJQ model, and in fact the effect of the quadrupole is of shorter range than the dispersion. Accordingly, the number of pairwise interactions is reduced from 64 for ethane (36 for ethylene) in the AA-OPLS model to 5 in the 2CLJQ model. Since the largest part of a molecular simulation time revolves around the calculation of these pairwise interactions, a reduction in the number of these calculations results directly in an increase of the corresponding computational speed.

In the limit of zero surface coverage, we estimated the Henry's constant, H, for both fluids using the 2CLJQ model, measuring the slopes of the isotherms in the near zero coverage region. As is expected at very low pressures, the adsorption as a function of pressure shows a linear relation with slopes of $\theta_{ethylene} = 710 \pm 1$ μmol m^{-2} bar^{-1} and $\theta_{ethane} = 2224 \pm 7$ μmol m^{-2} bar^{-1}, confirming the expected enhanced adsorption of ethane with respect to ethylene at low pressures. We have also determined the isosteric

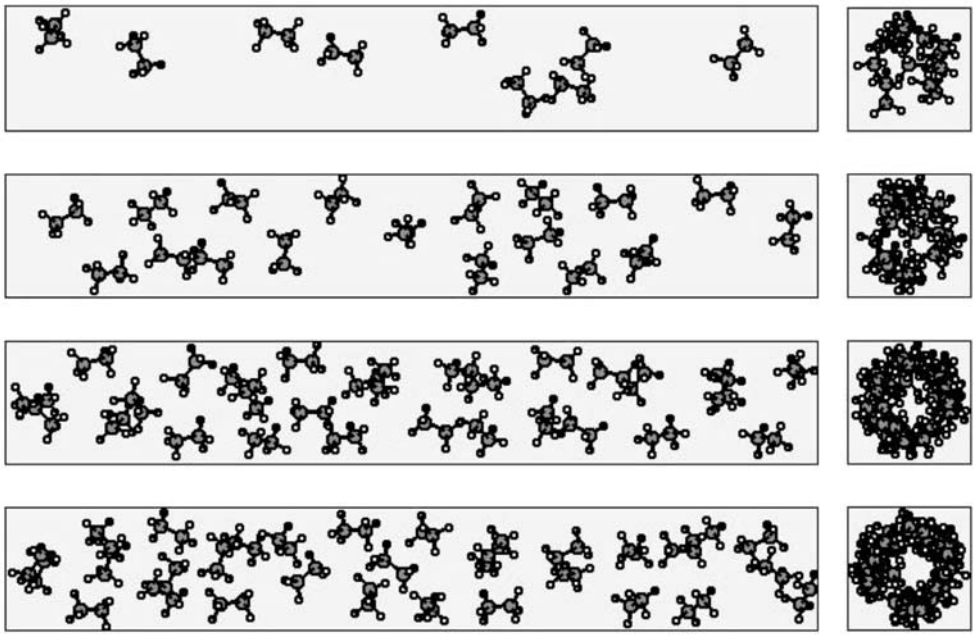

Fig. 4 Schematic representation of the effect of pressure on the loading capacity of ethane, at $T = 300$ K. From *top* to *bottom* the equilibrium bulk pressure is 0.28 bar, 1.45 bar, 11.7 bar and 25 bar respectively. Nanotube atoms have been deleted for clarity, and fluid molecules are represented in an arbitrary scale. Right hand side figures correspond to the view along the nanotube main axis

Table 3 Isosteric heats of adsorption for the 2CLJQ model at $T = 300$ K (6)

	q_{iso} $(-\Delta H)$/kJ mol^{-1}		
C_2H_4	6.22 (0.17)	8.61 (1.25)	11.35 (10.71)
C_2H_6	13.72 (0.12)	15.81 (1.25)	15.79 (11.12)

Values in parenthesis are the corresponding bulk pressures in bar

heats of adsorption for ethane and ethylene at $T = 300$ K using the 2CLJQ model, based on the definition given by Nicholson and Parsonage (1982) (6), where $\langle \cdots \rangle$ denotes the ensemble average, N is the number of particles, U is the system's configurational energy and k_B is the Boltzmann constant.

$$q_{iso} = \frac{\langle U \rangle \langle N \rangle - \langle UN \rangle}{\langle N^2 \rangle - \langle N \rangle \langle N \rangle} + k_B T \tag{6}$$

Results thus obtained are recorded in Table 3 and were determined extracting the last 5×10^6 cycles of GCMC data, thus making sure that equilibrium conditions had been attained. These results also indicate how at low pressure, ethane adsorption is slightly enhanced when comparing with the corresponding alkene. At $0.12 < p < 0.17$ bar, the alkane isosteric heat is roughly twice that of ethylene, indicating that ethane adsorption corresponds to a more thermodynamically stable process. As pressure increases, so does q_{iso}, but now the ethylene isosteric heat increases more rapidly than that for ethane, corroborating the idea that, as one moves towards the high pressure region, there will be a crossover of the isotherms, and ethylene will assume the role of the preferred adsorbed species.

In order to access the effect of nanotube geometry on the adsorption properties of these molecules, we have also performed simulations employing armchair, (9, 9), and chiral (12, 6) nanotubes who share similar diameters to the zig-zag (16, 0) nanotube used in the rest of the simulations. We have employed a similar length to diameter ratio of $(L/D) \approx 5.67$, and the same total number of AA-OPLS fluid particles in the simulation box. In all cases surface coverage data only deviated -3.4% to 7% compared to the zig-zag system, values characteristic of the intrinsic fluctuations associated with the MD technique. For all practical purposes, nanotube symmetry appears to be an irrelevant factor whenever adsorption properties are concerned. To study the influence of the available endohedral volume on the saturation capacity, a set of MD simulations was run, varying the effective volume available for the fluid molecules to be accommodated inside the tubes. Zig-zag nanotubes with diameters, D, of 4.46 Å, 6.80 Å, 11.49 Å, and 13.84 Å were put in contact with a bulk fluid at $p < 1$ bar. The results thus obtained are recorded in Fig. 5, where lines are parabolic functions fitted to simulation data; their zero-point derivative estimates an optimal value for gas storage located at $D_{optimal} \approx 9.5$ Å and $D_{optimal} \approx 10.0$ Å, for ethylene and ethane, respectively, indicating that ethane needs a slightly larger tube diameter to be suitably accommodated. For the narrowest nanotube studied, with a corresponding diameter of 4.46 Å, fluid molecules are almost incapable of accessing its interior volume thus resulting in a negligible adsorption. This is enhanced in the case of ethylene due to its planar geometry and rigid π bond, which contributes to make the molecule relatively stiff.

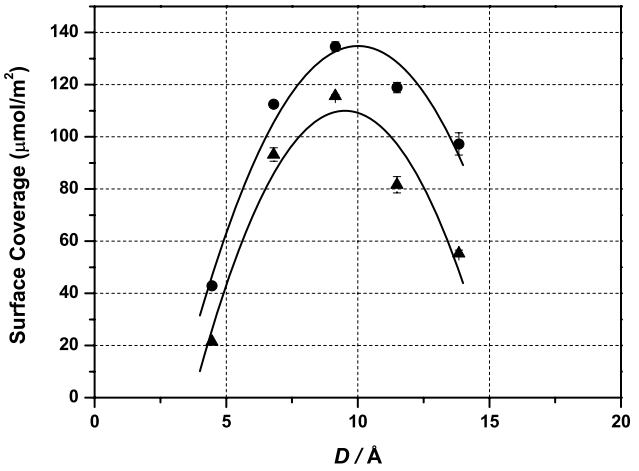

Fig. 5 Influence of the SWCNT diameter, D, on the surface coverage for ethylene (*triangles*) and ethane (*circles*), at $T = 300$ K. *Lines* are a guide to the eye

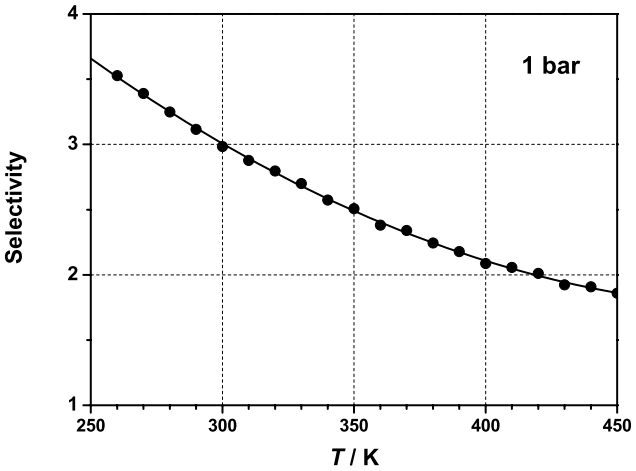

Fig. 6 Ethane selectivity, S, profile for a bulk fluid with 90 mol% ethylene at $p = 1$ bar

Table 4 Parameters for the Toth isotherm (7)

		C_2H_4		C_2H_6	
		AA-OPLS	2CLJQ	AA-OPLS	2CLJQ
Toth	$C_{\mu s}$/μmol·m^2	355.91	352.74	370.92	324.13
	b/bar^{-1}	0.641	2.852	1.577	11.233
	t	1.144	0.965	0.709	0.927

To fit simulation data we have employed the Toth equation (7), where $C_{\mu s}$ represents the saturation capacity in the high-pressure limit, and b is the so-called affinity constant.

$$C_\mu = C_{\mu s}\frac{bp}{[1+(bp)^t]^{1/t}} \tag{7}$$

Results thus obtained are recorded in Table 4 and graphically included in Fig. 3. A similar quality of fit was found with other semi-empirical isotherms, namely the Sips (Langmuir-Freundlich) model; their major difference being in the description of the system in the sub-monolayer regime, that is, in the low-pressure end (Do 1998; Rouquerol et al. 1998).

4.2 Binary mixtures

To study the separation of binary fluid mixtures of ethylene/ethane, we define a selectivity towards ethane as in (8), where x_i denotes the molar fraction of component i, and $(\ldots)_{pore}$ and $(\ldots)_{bulk}$ refers to the pore and bulk quantities, respectively.

$$S = \frac{(x_{ethane}/x_{ethene})_{pore}}{(x_{ethane}/x_{ethene})_{bulk}} \tag{8}$$

This way of probing separation involves the ratio between the molar fractions of the two components, confined in the pore and in the corresponding bulk gas. The results presented in this section correspond to the coarse grained 2CLJQ model. Even though there are quantitative differences between the adsorption curves predicted by the AA-OPLS model and the 2CLJQ models, the qualitative trends are similar, up to the point that one would expect that the ratio of competitive adsorption would be similar in both models.

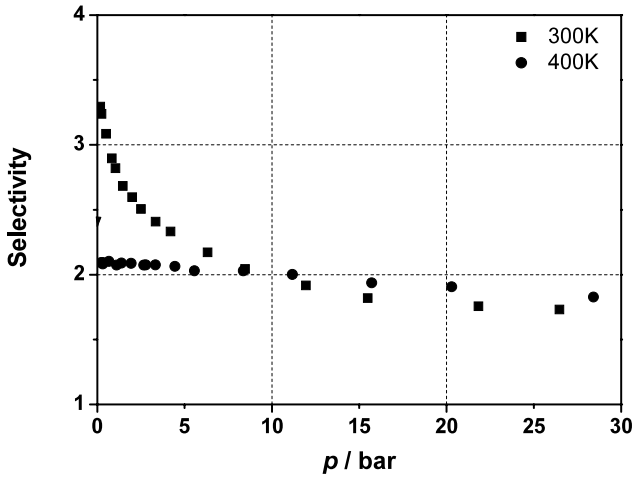

Fig. 7 Ethane selectivity, S, profiles for an equimolar mixture. *Squares* are for $T = 300$ K, and *circles* are for $T = 400$ K

Results were determined for two different kinds of binary fluid mixtures: i) a typical refinery feedstock mixture of 90 mol% ethylene at a total bulk pressure of $p = 1$ bar and in the temperature range 260 K $< T <$ 450 K, and ii) for an equimolar bulk mixture in the pressure range $0.1 < p <$ 30 bar at $T = 300$ K and $T = 400$ K. These data were obtained by averaging 5×10^6 cycles after equilibration runs of 25×10^6 GCMC cycles, and are plotted in Fig. 6 and Fig. 7.

For the 90% ethylene bulk fluid at 300 K the selectivity spans the range $2 < S < 4$, well in accordance with the simulation results obtained by Keil and Jakobtorweihen (2007) on larger diameter nanotubes and by Curbelo and Müller (2005) on carbon slit pores. It does appear that the unique 1-D geometry of the narrow nanotubes considered here is a relatively unimportant factor to be taken into account when industrially separating binary mixtures of C_2H_4/C_2H_6. At constant bulk pressure, we can observe a marked decrease of selectivity with the increase of temperature, almost by a factor of 50% (Fig. 6). High temperatures tend to reduce the energetic differences between molecules, and therefore it is not surprising that selectivity decreases sharply from $S = 3.53$ ($T = 260$ K) down to $S = 1.86$ ($T = 450$ K).

If temperature becomes a working variable in the separation process (Fig. 7), than two general remarks can be made. For the highest temperature studied, $T = 400$ K, selectivity decreases smoothly and always linearly with bulk fluid pressure, from a value of $S = 2.1$ down to $S = 1.6$. In the other temperatures studied, selectivity starts to decrease very rapidly up to a certain limiting bulk pressure ($p \approx 10$ bar), where it reaches a plateau: from then onwards it follows a linear behavior similar to the one observed at $T = 400$ K. In all cases, the higher selectivity values coincides with the low pressure regions, where ethane is the preferentially adsorbed species.

5 Conclusions

Both the AA-OPLS and the 2CLJQ models present the same features for the adsorption isotherms of pure ethane and ethylene on small diameter nanotubes, although the results do not match quantitatively, particularly in the vicinity of ambient pressure. As pressure increases, from $p \approx 10$ bar onwards, both force-fields predict similar results. No comparison is yet possible with experimental data, and even if these were available, the most likely scenario would require a manual adjustment (fitting) of the solid-fluid interaction parameters. Thus, for all practical purposes, and taking into the account the reduced computer CPU time needed by the coarse grained model, the latter is recommended for any further adsorption study, particularly where intermediate and high pressures need to be addressed.

Results showed a threshold (crossover) pressure, in the lower vicinity of 10 bar, below which ethane molecules are preferentially adsorbed over ethylene. Selectivity is not large, typically below $S = 4$. This preferential ethane adsorption is attributed to the larger dispersive forces that characterize the ethane molecules, and verified by the calculation of the corresponding isosteric heats of adsorption (Table 3) and low coverage Henry's constants. Nanotube geometry plays a minor role on the adsorption properties, which seem to be driven at lower pressures primarily by the larger affinity of the alkane towards the carbon surface and at higher pressures by packing effects. The fact that the selectivity towards ethane is similar to that found earlier on carbon slit pores and larger diameter nanotubes, points to the fact that the peculiar 1-D geometry of the nanotubes poses no particular incentive for the selective adsorption of either species.

Acknowledgements The authors would like to thank Dr. I.A.A.C. Esteves (*Universidade Nova de Lisboa*, *Portugal*), for helpful comments. This work has been supported by the Engineering and Physical Sciences Research Council of the UK through Grant EP/D035171.

References

Ackerman, D.M., Skoulidas, A.I., Sholl, D.S., Johnson, J.K.: Diffusivities of Ar and Ne in carbon nanotubes. Mol. Sim. **29**, 677–684 (2003)

Agnihotri, S., Mota, J.P.B., Rostam-Abadi, M., Rood, M.J.: Theoretical and experimental investigation of morphology and temperature effects on adsorption of organic vapors in single-walled carbon nanotubes. J. Phys. Chem. B **110**, 7640–7647 (2006)

Al-Baghli, N.A., Loughlin, K.F.: Binary and ternary adsorption of methane, ethane, and ethylene on titanosilicate ETS-10 zeolite. J. Chem. Eng. Data **51**, 248–254 (2006)

Alba-Simionesco, C., Coasne, B., Dosseh, G., Gubbins, K.E., Radhakrishnan, R., Sliwinska-Bartkowiac, M.: Effects of confinement on freezing and melting. J. Phys., Condens. Matter **18**, R15–R68 (2006)

Allen, M.P., Tildesley, D.J.: Computer Simulation of Liquids. Clarendon Press, Oxford (1990)

Bekyarova, E., Murata, K., Yudasaka, M., Kasuya, D., Iijima, S., Tanaka, H., Kahoh, H., Kaneko, K.: Single-wall nanostructured carbon for methane storage. J. Phys. Chem. B **20**, 4681–4684 (2003)

Bethune, D.S., Kiang, C.H., Vries, M.S.D., Gorman, G., Savoy, R., Vasquez, J., Beyers, R.: Cobalt-catalysed growth of carbon nanotubes with single-atomic-layer walls. Nature **363**, 605–607 (1993)

Carrero-Mantilla, J., Llano-Restrepo, M.: Further validation of a set of quadrupolar potential models for ethylene and propylene from the prediction of some binary mixture vapor–liquid equilibria by Gibbs-ensemble molecular simulation. Mol. Sim. **29**, 549–554 (2003)

Chacin, A., Vazquez, J.M., Müller, E.A.: Molecular simulation of the Joule-Thomson inversion curve of carbon monoxide. F. Phase Eq. **165**, 147–155 (1999)

Choi, B.U., Choi, D.-K., Lee, Y.-W., Lee, B.-K., Kim, S.-H.: Adsorption equilibria of methane, ethane, ethylene, nitrogen, and hydrogen onto activated carbon. J. Chem. Eng. Data **48**, 603–607 (2003)

Cracknell, R.F., Nicholson, D.: Grand canonical Monte Carlo study of Lennard-Jones mixtures in slit pores. Part 3. Mixtures of two molecular fluids: ethane and propane. J. Chem. Soc., Faraday Trans. **90**, 1497–1493 (1994)

Curbelo, S., Müller, E.A.: Modelling of ethane/ethylene separation using microporous carbon. Ads. Sci. Tech. **23**, 855–865 (2005)

Da Silva, F.A., Rodrigues, A.E.: Adsorption equilibria and kinetics for propylene and propane over 13X and 4A zeolite pellets. Ind. Eng. Chem. Res. **38**, 2051–2057 (1999)

Darkrim, F.L., Malbrunot, P., Tartaglia, G.P.: Review of hydrogen storage by adsorption in carbon nanotubes. Int. J. Hyd. Energy **27**, 193–202 (2002)

Daubert, T.E., Danner, R.P.: Physical and Thermodynamic Properties of Pure Chemicals, 4th edn. Taylor and Francis, London (1994)
Do, D.D.: Adsorption Analysis and Kinetics. Imperial College Press, London (1998)
Do, D.D., Do, H.D.: Effects of potential models on the adsorption of ethane and ethylene on graphitized thermal carbon black. Study of two-dimensional critical temperature and isosteric heat versus loading. Langmuir **25**, 10889–10899 (2004a)
Do, D.D., Do, H.D.: Adsorption of ethylene on graphitized thermal carbon black and in slit pores: a computer simulation study. Langmuir **20**, 7103–7116 (2004b)
Do, D.D., Do, H.D.: Cooperative and competitive adsorption of ethylene, ethane, nitrogen and argon on graphitized carbon black and in slit pores. Adsorption **11**, 35–50 (2005)
Düren, T., Keil, F.J., Seaton, N.A.: Molecular simulation of adsorption and transport diffusion of model fluids in carbon nanotubes. Mol. Phys. **100**, 3741–3751 (2002)
Fagan, J.A., Simpson, J.R., Bauer, B.J., De Paoli Lacerda, S.H., Becker, M.L., Chun, J., Migler, K.B., Walker, A.R.H., Hobbie, E.K.: Length-dependent optical effects in single-wall carbon nanotubes. J. Am. Chem. Soc. **129**, 10607–10612 (2007)
Fernández, G.A., Vrabec, J., Hasse, H.: Shear viscosity and thermal conductivity of quadrupolar real fluids from molecular simulation. Mol. Sim. **31**, 787–793 (2005a)
Fernández, G.A., Vrabec, J., Hasse, H.: Self-diffusion and binary Maxwell–Stefan diffusion coefficients of quadrupolar real fluids from molecular simulation. Int. J. Therm. **26**, 1389–1407 (2005b)
Frenkel, D., Smit, B.: Understanding Molecular Simulation, 2nd edn. Academic Press, San Diego (2002)
Funk, S., Burghaus, U., White, B., O'Brien, S., Turro, N.J.: Adsorption dynamics of alkanes on single-wall carbon nanotubes: a molecular beam scattering study. J. Phys. Chem. C **111**, 8043–8049 (2007)
Gelb, L.D., Gubbins, K.E., Radhakrishnan, R., Sliwinska-Bartkowiak, M.: Phase separation in confined systems. Rep. Prog. Phys. **62**, 1573–1659 (1999)
Gray, C.G., Gubbins, K.E.: Theory of Molecular Fluids. Clarendon Press, Oxford (1984)
Guo, J., Bao, X.T., Gui, B., Xiang, S.X., Li, S.R., Huang, X.F., Heslop, M.J.: Co-adsorption equilibrium of ethane and ethylene mixture onto various activated carbons. Paper presented in FOA9 Naxos, Italy, 2007
Heyden, A., Düren, T., Keil, F.J.: Study of molecular shape and non-ideality effects on mixture adsorption isotherms of small molecules in carbon nanotubes: a grand canonical Monte Carlo simulation study. Chem. Eng. Sci. **57**, 2439–2448 (2002)
Hong, S.Y., Tobias, G., Ballesteros, B., Oualid, F.E., Errey, J.C., Doores, K., Kirkland, A.I., Nellist, P.D., Green, M.L.H., Davis, B.G.: Atomic-scale detection of organic molecules coupled to single-walled carbon nanotubes. J. Am. Chem. Soc. **129**, 10966–10967 (2007)
Hung, F.R., Coasne, B., Santiso, E.E., Gubbins, K.E., Siperstein, F.R., Sliwinska-Bartkowiak, M.: Molecular modeling of freezing of simple fluids confined within carbon nanotubes. J. Chem. Phys. **122**, 144706(144701)–144706(144714) (2005)
Iijima, S.: Helical microtubules of graphitic carbon. Nature **354**, 56–58 (1991)
Iijima, S., Ichihashi, T.: Single-shell carbon nanotubes of 1-nm diameter. Nature **363**, 603–605 (1993)
IUPAC: Reporting physisorption data for gas/solid isotherms. Pure Appl. Chem. **57**, 603–619 (1985)
Jiang, J., Sandler, S.I.: Capillary phase transitions of linear and branched alkanes in carbon nanotubes from molecular simulation. Langmuir **22**, 7391–7399 (2006)
Jiang, J., Wagner, N.J., Sandler, S.I.: A Monte Carlo simulation study of the effect of carbon topology on nitrogen adsorption on graphite, a nanotube bundle, C60 fullerite, C168 schwarzite, and a nanoporous carbon. Phys. Chem. Chem. Phys. **6**, 4440–4444 (2004)
Jiang, J., Sandler, S.I., Schenk, M., Smit, B.: Adsorption and separation of linear and branched alkanes on carbon nanotube bundles from configurational-bias Monte Carlo simulation. Phys. Rev. B **72**, 45447 (2005)
Jorgensen, W.L., Maxwell, D.S., Tirado-Rives, J.: Development and testing of the OPLS all-atom force field on conformational energetics and properties of organic liquids. J. Am. Chem. Soc. **118**, 11225–11236 (1996)
Kaneko, K., Cracknell, R.F., Nicholson, D.: Nitrogen adsorption in slit pores at ambient temperatures: comparison of simulation and experiment. Langmuir **10**, 4506–4609 (1994)
Keil, F.J., Jakobtorweihen, S.: Adsorption and diffusion of alkanes and alkenes in carbon nanotubes. Paper presented in AIChE Annual Meeting Salt Lake City, USA, 2007
Klochko, A.V., Brodskaya, E.N., Piotrovskaya, E.M.: Computer simulations of dependence of adsorption characteristics of ethane on the size of graphite micropores. Langmuir **15**, 545–552 (1999)
Kondratyuk, P., Wang, Y., Johnson, J.K., Yates, J.T., Jr.: Observation of a one-dimensional adsorption site on carbon nanotubes: adsorption of alkanes of different molecular lengths. J. Phys. Chem. B **109**, 20999–21005 (2005)
Leach, A.R.: Molecular Modeling Principles and Applications. Longman, London (1996)
Liu, Y., Gao, L., Sun, J., Zheng, S., Jiang, L., Wang, Y., Kajiura, H., Li, Y., Noda, K.: A multi-step strategy for cutting and purification of single-walled carbon nanotubes. Carbon **45**, 1972–1978 (2007)
Longhurst, M.J., Quirke, N.: Temperature-driven pumping of fluid through single-walled carbon nanotubes. Nano Lett. **7**, 3324–3328 (2007)
Lu, J.Q., Rider, D.A., Onyegam, E., Wang, H., Winnik, M.A., Manners, I., Cheng, Q., Fu, Q., Liu, J.: Carbon nanotubes with small and tunable diameters from poly(ferrocenylsilane)-block-polysiloxane diblock copolymers. Langmuir **22**, 5174–5179 (2006)
Mao, Z., Sinnott, S.B.: Separation of organic molecular mixtures in carbon nanotubes and bundles: molecular dynamics simulations. J. Phys. Chem. B **105**, 6916–6924 (2001)
McDonald, N.A., Carlson, H.A., Jorgensen, W.L.: Free energies of solvation in chloroform and water from a linear response approach. J. Phys. Org. Chem. **10**, 563–576 (1997)
Meyyappan, M.: Carbon Nanotubes: Science and Applications. CRC Press, London (2005)
Mukherjee, B., Maiti, P.K., Dasgupta, C., Sood, A.K.: Strong correlations and Fickian water diffusion in narrow carbon nanotubes. J. Chem. Phys. **126**, 124704–124711 (2007)
Nicholson, D., Parsonage, N.G.: Computer Simulation and the Statistical Mechanics of Adsorption. Academic Press, New York (1982)
NIST (2008). Chemistry Webbook. http://webbook.nist.gov
Noble, R.D., Agrawal, R.: Separations research needs for the 21st century. Ind. Eng. Chem. Res. **44**, 2887–2892 (2005)
Nosé, S.: A unified formulation of the constant temperature molecular dynamics methods. J. Chem. Phys. **81**, 511–519 (1984)
Ohba, T., Kaneko, K.: Internal surface area evaluation of carbon nanotube with GCMC simulation-assisted N_2 adsorption. J. Phys. Chem. B **106**, 7171–7176 (2002)
Rouquerol, F., Rouquerol, J., Sing, K.: Adsorption by Powders and Porous Media. Academic Press, New York (1998)
Rowlinson, J.S., Swinton, F.L.: Liquids and Liquid Mixtures. Butterworths, London (1982)
Saito, R., Dresselhaus, G., Dresselhaus, M.S.: Physical Properties of Carbon Nanotubes. Imperial College Press, London (1998)
Simonyan, V.V., Diep, P., Johnson, J.K.: Molecular simulation of hydrogen adsorption in charged single-walled carbon nanotubes. J. Chem. Phys. **111**, 9778–9783 (1999)

Simonyan, V.V., Johnson, J.K., Kuznetsova, A., Yates, J.T.: Molecular simulation of xenon adsorption on single-walled carbon nanotubes. J. Chem. Phys. **114**, 4180–4185 (2001)

Sinnott, S.B., Andrews, R.: Carbon nanotubes: synthesis, properties, and applications. Crit. Rev. Sol. State Mat. Sci. **26**, 145–249 (2001)

Skoulidas, A.I., Sholl, D.S., Johnson, J.K.: Adsorption and diffusion of carbon dioxide and nitrogen through single-walled carbon nanotube membranes. J. Chem. Phys. **124**, 54708(54701)–54708(54707) (2006)

Smith, W., Todorov, I.T.: A short description of DL_POLY. Mol. Sim. **32**, 935–943 (2006)

Solomons, T.W.: Organic Chemistry, 5th edn. Wiley, New York (1992)

Steele, W.A.: The physical interactions of gases with crystalline solids. Surf. Sci. **36**, 317–352 (1973)

Steele, W.A.: The Interaction of Gases with Solid Surfaces. Pergamon Press, Oxford (1974)

Steele, W.A.: Molecular interactions for physical adsorption. Chem. Rev. **93**, 2355–2378 (1993)

Stoll, J., Vrabec, J., Hasse, H.: Vapor–liquid equilibria of mixtures containing nitrogen, oxygen, carbon dioxide, and ethane. AIChE J. **49**, 2187–2198 (2003)

Striolo, A., Chialvo, A.A., Gubbins, K.E., Cummings, P.T.: Water in carbon nanotubes: adsorption isotherms and thermodynamic properties from molecular simulation. J. Chem. Phys. **122**, 234712(234711)–234712(234714) (2005)

Sweatman, M.B., Quirke, N., Zhu, W., Kapteijn, F.: Analysis of gas adsorption in kureha active carbon based on the slit–pore model and Monte-Carlo simulations. Mol. Sim. **32**, 513–522 (2006)

Taherpour, A.: Structural relationship between degree of unsaturation with polarizability of (5,5) armchair single-wall carbon nanotubes. Nanotubes Carbon Nanostruct. **15**, 279–289 (2007)

van Gunsteren, W.F., Berendsen, H.J.C.: Computer simulation of molecular dynamics: methodology, applications, and perspectives in chemistry. Angew. Chem. Int. Ed. Engl. **29**, 992–1023 (1990)

Verlet, L.: Computer "Experiments" on classical fluids. Thermodynamical properties of Lennard-Jones molecules. Phys. Rev. **159**, 98–103 (1967)

Vernov, A., Steele, W.A.: The electrostatic field at a graphite surface and its effect on molecule-solid interactions. Langmuir **8**, 155–159 (1992)

Vrabec, J., Stoll, J., Hasse, H.: A set of molecular models for symmetric quadrupolar fluids. J. Phys. Chem. B **105**, 12126–12133 (2001)

Vrabec, J., Kedia, G.K., Hasse, H.: Prediction of Joule–Thomson inversion curves for pure fluids and one mixture by molecular simulation. Cryogenics **45**, 253–258 (2005)

Woodcock, L.V., Singer, K.: Thermodynamics and structural properties of liquid ionic salts obtained by Monte Carlo computation. Trans. Farad. Soc. **67**, 12–30 (1971)

Yang, R.T.: Adsorbents: Fundamentals and Applications. Wiley, New Jersey (2003)

Yerushalmi-Rozen, R., Szleifer, I.: Utilizing polymers for shaping the interfacial behavior of carbon nanotubes. Soft. Matter. **2**, 24–28 (2006)

Zhao, X., Johnson, J.K.: An effective potential for adsorption of polar molecules on graphite. Mol. Sim. **31**, 1–10 (2005)